The origin and role of biological rock crusts in rocky desert weathering

Running title: Origin and role of BRC in arid rock weathering

Authors:

Nimrod Wieler[1], Hanan Ginat[2], Osnat Gillor[1]*[#] and Roey Angel[3]*[#]

* These authors contributed equally to this study

Affiliations

[1]Zuckerberg Institute for Water Research, Blaustein Institutes for Desert Research, Ben Gurion University of the Negev Sede Boqer Campus, Israel

[2]The Dead Sea and Arava Science Center, Israel

[3]Soil and Water Research Infrastructure and Institute of Soil Biology, Biology Centre CAS, Czechia

[#] Corresponding authors:

Roey Angel, Soil and Water Research Infrastructure and Institute of Soil Biology, Biology Centre CAS, Czechia. Phone: +420-387-775847; e-mail: roey.angel@bc.cas.cz

Osnat Gillor, Zuckerberg Institute for Water Research, Blaustein Institutes for Desert Research, Ben Gurion University of the Negev Sede Boqer Campus, Israel. Phone: +972-8-6596986; e-mail: gilloro@bgu.ac.il

Highlights/significance:

- Tafoni (honeycomb) weathering patterns were observed at similar frequency and magnitude in hard lime and dolomitic rocks originating from arid and hyperarid environments, respectively, despite different lithologies and climate.
- In drylands, rock surfaces are colonised by an epilithic microbial community, dominated by bacteria that form a biological rock crusts.
- The microbial communities on the hard lime and dolomitic rocks were dominated by members of the phyla Proteobacteria and Actinobacteria that are typical to drylands.
- The two BRC communities were nevertheless distinct from each other, but also from the surrounding soil and dust, showing the habitat filtering effect of the rock surfaces.
- Microbial and geological tools applied in this study suggest that in drylands biological rock crusts mitigate rock weathering processes by forming an evaporation barrier.

Keywords: Arid; Cavernous weathering; Biological rock crust (BRC); Microbiome; Calcrete; Dolocrete; Stable isotopes; FTIR; High-throughput sequencing

Abstract

In drylands, microbes that colonise rock surfaces were linked to erosion because water scarcity excludes traditional weathering mechanisms. We studied the origin and role of rock biofilms in geomorphic processes of hard lime and dolomitic rocks that feature comparable weathering morphologies though originating from arid and hyperarid environments, respectively. We hypothesised that weathering patterns are fashioned by salt erosion and mediated by the rock biofilms that originate from the adjacent soil and dust. We used a combination of microbial and geological techniques to characterise rocks morphologies and the origin and diversity of their biofilm. Amplicon sequencing of the SSU rRNA gene suggested that bacterial diversity is low and dominated by Proteobacteria and Actinobacteria. These phyla formed laminar biofilms only on rock surfaces that were exposed to the atmosphere and burrowed up to 6 mm beneath the surface, protected by sedimentary deposits. Unexpectedly, the microbial composition of the biofilms differed between the two rock types and was also distinct from the communities identified in the adjacent soil and settled dust, showing a habitat-specific filtering effect. Moreover, the rock bacterial communities were shown to secrete extracellular polymeric substances that form an evaporation barrier, reducing water loss rates by 65-75%. The reduced water transport rates through the rock also limit salt transport and its crystallisation in surface pores, which is thought to be the main force for weathering. Concomitantly, the biofilm layer stabilises the rock surface via coating and protects the weathered front. Our hypothesis contradicts common models, which typically consider biofilms as weathering-promoting agents. In contrast, we propose the microbial colonisation of mineral surfaces acts to mitigate geomorphic processes in hot, arid environments.

Introduction

In arid and hyperarid stony deserts, bedrock surfaces are typically barren and free of vegetation or continuous soil mantle. When these surfaces are exposed to atmospheric conditions, they undergo weathering processes that shape the landscape (Smith, 2009). Weathering is an in-situ set of processes that include physical, chemical and mechanical forces that result in the breakdown and transport of the shuttered fragments from the parent rock. Weathering can appear in a range of sizes and morphologies (Smith, Warke, McGreevy, & Kane, 2005), including gravel shattering (Amit, Harrison, Enzel, & Porat, 1996), surface crazing (Smith, 1988), ventifacts (Smith, 1988), microrills (Smith, 1988; Sweeting & Lancaster, 1982) and cavernous patterns [also known as tafoni, honeycomb or pitting (Mustoe, 1983; Viles, 2005)]. Weathering is an essential, though often neglected, element in the overall denudation of hot deserts.

Cavernous weathering is one of the most frequently occurring weathering patterns that have been observed in various regions across the globe, including humid and arid, cold and hot, coastal and inland sites (Bruthans, Filippi, Slavík, & Svobodová, 2018). In the Negev Desert, Israel, cavernous weathering patterns are common in carbonate rocks in arid and hyperarid regions. Upon exposure to the atmosphere, these rocks develop a carbonate coating, termed calcrete or dolocrete (respective to limestone or dolomite) by displacive and replacive cementation of calcium or dolomite onto the rock surface (Wright & Wacey, 2004; Alonso-Zarza & Wright, 2010). Following the cementation processes, typical honeycomb features are formed on the exposed parent rock, typified by pits separated by thin walls that are coated by the calcrete or dolocrete. Recent studies suggest that microbial activity also promotes the processes of calcrete and dolocrete formation (Alonso-Zarza & Wright, 2010; Alonso-Zarza, Bustamante, Huerta, Rodríguez-Berriguete, & Huertas, 2016).

The accepted conceptual model for the formation of cavernous rock weathering in hot deserts involves the presence of permeable rocks that are subjected to soluble salts and repeated episodes of drying-rewetting cycles (Goudie, Wright, & Viles, 2002; Smith, 1988; Smith et al., 2005). The proposed mechanisms assume that cavernous weathering results from physicochemical processes including salt crystallization (Cooke, 1979; Scherer, 2004), incipient fractures (Amit et al., 1996), exfoliation (Shtober-Zisu, Amasha, & Frumkin, 2017), or stress-erosion (Bruthans et al., 2014; McArdle & Anderson, 2001). Recently, Bruthans and colleagues (2018) conclusively demonstrated the superiority of the hydraulic hypothesis (moisture flux followed by salt crystallisation at the boundary layer) over case hardening model, in a temperate climate.

In addition, biological mechanisms have been proposed to promote rock weathering through mechanisms such as flaking via colony growth (Heather A. Viles, 2012), acidification by bacterial extractions (Garcia-Pichel, 2006; Warscheid & Braams, 2000) or alkalization during photosynthesis by cyanobacteria (Büdel et al., 2004). In contrast, it was proposed that micro- and macro-organisms colonisation can mitigate weathering in temperate, coastal regions (McIlroy de la Rosa, Warke, & Smith, 2014; George E. Mustoe, 2010) through encrustation or protection from direct rain impact. Yet, it is not clear which of these mechanisms dominates or what is the relative contribution of chemical vs biological processes to weathering in arid environments.

Microorganisms colonising rocks form a hardy biofilm known as the biological rock crusts (BRC), which is common in most arid and hyperarid regions worldwide (Gorbushina, 2007; Lebre, Maayer, & Cowan, 2017; Pointing & Belnap, 2012). Epilithic communities colonising rock surfaces are ubiquitous in arid environments, while hyperarid rocks, which experience increased radiation and desiccation, are dominated by endolithic communities that colonise internal rock pores (Makhalanyane et al., 2013; Pointing & Belnap, 2012; Viles, 1995). The BRC communities include cyanobacteria and other phototrophic bacteria and heterotrophic bacteria, but very low

abundances of archaea, fungi or algae (Lang-Yona et al., 2018). However, the BRC inoculum was not resolved and was proposed to originate from settled dust (Viles, 2008), or the surrounding soil (Makhalanyane et al., 2015).

The goal of this study was to illuminate the origin and role of BRCs in cavernous weathering of exposed limestone and dolomite rocks in arid and hyperarid regions. We predicted that the BRC communities on exposed rock surfaces will resemble either the ever-present dust or the surrounding soil, supporting a subset of adapted taxa from both sources. We further hypothesised that the cavernous weathering morphologies of exposed rocks result from salt mobilisation by dew, causing crystallisation pressure under atmospheric conditions. The developed rock biofilms clog the surface rock pores through secretion of extracellular polymeric substances (EPS), lowering evaporation and slowing the salt crystallisation, but also stabilising the exfoliated rocks preventing further weathering. Thus, the presence of a BRC mitigates the geomorphic processes. To test our hypotheses, we applied a holistic approach combining field observations, geological, geotechnical and molecular microbiology characterisation elucidating BRCs' morphology, origin and role in arid cavernous weathering.

Results and discussion

Field and mineralogical observations

Weathering features were observed in about 30% of exposed rocks sampled from both arid and hyperarid sites. Neither the prevalence of weathering nor its morphology seemed to differ between sites despite the different climates and underlying geology. In all cases, weathering type was classified as tafoni or honeycomb weathering (Goudie, Viles, & Parker, 1997; Groom, Allen, Mol, Paradise, & Hall, 2015; Fig. 1A), and it was coupled with the presence of sub-aerial biofilm, burrowed underneath the surface and protected by sedimentary deposits (Fig. 1B). The weathering and presence of the crusts were restricted to the atmospherically exposed parts of the rock. The presence of identical weathering morphology and prevalence in different climates and lithologies challenges the current model, which assumes that surface permeability, moisture and the presence of salts as primary factors control weathering rates (Andrew S. Goudie et al., 2002; Smith, 1988; Smith et al., 2005). However, the lack of correlation between tafoni weathering magnitude and climate has already been reported (Brandmeier, Kuhlemann, Krumrei, Kappler, & Kubik, 2011).

To study the possible differences between these sites, we performed geological characterisation of 10 limestone and dolomite rocks collected from the arid and hyperarid sites, respectively, testing for mineral content, porosity, permeability and elasticity. As expected, our results showed different lithological parameters between the limestone and dolomite rocks (Table 1), yet they displayed similar weathering features. Moreover, petrographic thin section analysis showed that on both rock types, crusts had developed to a similar thickness of 1-6 mm, irrespective of climatic conditions including mean annual precipitation (Fig. 1C). However, microclimatic conditions, like dew or surface temperature may impact local morphologies. Also, the thin sections showed that the crusts are composed of masses of micritic to microsparitic minerals that form laminated structure (Fig.

1C). Such laminated structures indicate that the crusts are stage four terrestrial calcretes and dolocretes, suggesting a mature crust phase (Alonso-Zarza & Wright, 2010). The calcretes and dolocretes identified on the rocks' surface reject previously suggested impact of mineralised networks or case hardening (McBride & Picard, 2004). In fact, the detection of mature calcretes could serve as an indication of atmospheric exposure but was also suggested to result from biogenic activity (Alonso-Zarza & Wright, 2010; Goudie, 1996).

Composition and chemical characteristics of the rock crusts

To test our hypothesis that the crusts are biogenic and involved in rock weathering processes, we characterised their origin and nature. An XRD analysis of the crust layers and bedrocks showed that the crusts are composed of similar mineralogy as their respective host rocks, indicating that local weathering, rather than dust deposition, is the source of crust generation (Table 1).

The biogenic nature of the crusts was confirmed using a cross-section analysis of the stable carbon and oxygen isotopes ratios in the crust and host rock (Fig. 2A). For both limestone and dolomite, values of $\delta^{13}C$ increased between the crust and the host rock layers and ranged from -4.1‰ in the calcrete to -0.9‰ in the limestone bed, and from 0.2‰ in the dolocrete to 2.0‰ in the dolomite bed. Such values are typical indicators to carbon isotope exchange of primary marine $CaCO_3$ (abundant in the bedrock) with CO_2 released by microbial respiration (i.e. of carbon originating from photosynthesis) with subsequent precipitation of pedogenic calcrete (Brlek & Glumac, 2014; Mora, Driese, & Seager, 1991). Analysing $\delta^{13}C$, together with $\delta^{18}O$, compositions of pedogenic carbonates is a useful way of reconstructing paleo-vegetation (e.g., C3/C4 plant ratio; Ehleringer, Cerling, & Helliker, 1997; Mora et al., 1991). Our $\delta^{13}C$ results go along with $\delta^{13}C$ values collected from speleothems (secondary mineral deposits formed in caves) collected in the central and southern Negev Desert (Vaks, Bar-Matthews, Matthews, Ayalon, & Frumkin, 2010) that were

also dated to end of the Pliocene (the past 2.5 million years). The low ratio detected here (Fig 2A) and by Vaks et al. (2010) suggest that the Negev region has been able to support only limited vegetation for at least 2.5 Ga, if so then the role of the crust in shaping the morphology of the rock surfaces was considerable. These results support the hypothesis that calcretes and dolocretes are of biogenic origin, and therefore the crust can be referred to as BRC. Moreover, they indicate similar developmental trajectory for both the calcretes and dolocretes that is independent of aridity or lithological parameters.

In contrast, the trend in values of $\delta^{18}O$ differed between rock types. In the limestone rocks, the ratio ranged from -3.0‰ to -6.8‰ between the BRC and the host rock, while in the dolomite it was higher, ranging from -5.4‰ to -0.6‰. The decrease in $\delta^{18}O$ in the host limestone rock could be explained by meteoric water substitution (Sandler, 2006). In contrast, the more negative $\delta^{18}O$ values in the dolocrete compared to the host dolomite are attributed to isotopic differentiation of meteoric water due to condensation (Rayleigh distillation) and could result from the large distance from the Mediterranean Sea (that is the primary source of rainfall in the area) compared to closer limestone rocks. In speleothems, similar patterns in $\delta^{18}O$ values were reported in the central and southern Negev Desert (Vaks et al., 2010). The results suggest that the calcrete and dolocrete studied here have been experiencing arid to hyperarid climates since the Pleistocene, alluding to the possible source of rain. A similar study conducted in the Thar Desert in India also inferred sedimentary rocks stable isotope patterns to paleoclimate (Andrews et al., 1998).

To study the potential role of the BRC in the weathering process, its composition was characterised using FTIR as was previously reported (Sheng, Yu, & Li, 2010). We focused on the functional groups and element compositions in EPS or microbial aggregates and found a distinct peak in the BRC layers ranging between 1020-1040 cm^{-1} in both limestone and dolomite rocks that was absent from the host rocks (Fig. 2B). This peak is indicative of the presence of EPS from

bacterial origin (Shirshova, Ghabbour, & Davies, 2006), pointing to the significant components of asymmetric and symmetric stretching of PO_2^- and $P(OH)_2$ in phosphate as well as vibrations of C-OH and C-C bonds found in polysaccharides and alcohols (Jiang et al., 2004). These results provide a strong support for the biogenic nature of the crust, since EPS is a common feature of many if not most biofilms (Drews, Lee, & Kraume, 2006). The detected EPS could serve several functions in BRC such as dust-particle trap to collect the dust and its nutrients, a binding agent to individual members of the biofilm (Davey & O'toole, 2000), or a protective agent by decreasing evaporation and retaining moisture and shielding from radiation (Or, Smets, Wraith, Dechesne, & Friedman, 2007; Roberson & Firestone, 1992).

Based on these findings, we hypothesised that BRC could in fact act as a mitigator during the weathering process by clogging the pores on the surface of the rock and thereby minimising capillary rise. Consequently, crystallisation of dissolved salts, considered to be the primary mechanism for rock weathering, is mitigated. To test this hypothesis, we performed a desiccation experiment to estimate water loss from the rock surfaces covered with BRC. The results suggest that both in limestone and dolomite rocks water moves through the rock and is lost to evaporation two or three times faster in the absence of BRC than when it is present (Fig. 3). Considering that salt transport due to hydraulic movement is a dominant weathering mechanism (Huinink, Pel, & Kopinga, 2004), reduced evaporation due to BRC coverage will also inevitably lead to decrease weathering rate. Moreover, the obtained results stand in contrast to similar measurements performed on temperate sandy stones that showed no significant effect of BRC on water transport rates (Slavík et al., 2017).

The microbial composition and origin of the BRCs

To elucidate the identity of the bacterial communities on the limestone and dolomite BRCs, we applied a multiplexed barcoded amplicon sequencing of the small subunit RNA gene (SSU rRNA). In addition, we compared the BRC communities to those of samples of the surrounding soil and settled dust in order to deduce the origin for the rock biofilm. As expected, we found poor and low-diversity of the BRC communities. The communities of the BRC showed an average of 182 and 129 observed, 354 and 315 predicted phylotypes, and Shannon's H was 3.8 and 3.3 (Fig. 4A; Table S2), for arid limestone and hyperarid dolomite, respectively, with no significant difference between the rock types.

The surrounding soil was significantly richer and more diverse ($P < 0.05$) in the arid site (416 and 746 observed and predicted OTUs and Shannon's H = 5.6 on average), and equally rich but slightly more diverse in the hyperarid site (221 and 466 observed and predicted OTUs and Shannon's H = 3.8, on average. The diversity of the dust samples were was as poor as the BRC's (169 and 107 observed and predicted OTUs and Shannon's H = 3.0 and 1.5, on average) and did not differ between sites (Fig. 4A; Table S2). The number of observed OTUs in the soil and their diversity scores were somewhat lower in this study compared to reports from similar environments (Barberán, Henley, Fierer, & Casamayor, 2014; Šťovíček, Kim, Or, & Gillor, 2017) however these could be due to sequencing technologies and depth. The lower richness and diversity in hyperarid vs arid samples and the BRC and dust vs. soil samples is expected and comparable with trends reported in other works (Angel & Conrad, 2013; Barberán et al., 2014; Lang-Yona et al., 2018).

Beta-diversity analysis showed statistically significant differences between samples on the OTU-level by climate, sample type, and to a small extent also their interaction, using variance partitioning. These parameters were found to significantly contribute to the differences in bacterial communities accounting for 22%, 40% and 3.8% of the variance (Fig. 4B, Table S3). Pairwise comparisons further showed that the two BRCs significantly differed from one another ($P < 0.01$)

and also from their surrounding soil and dust samples ($P < 0.05$ in all cases; Table S3). The bacterial community in the samples was typical for drylands, mostly dominated by members of the phyla Proteobacteria, and Actinobacteria followed by Deinococcus–Thermus, Chloroflexi, Bacteroidetes, Cyanobacteria, Acidobacteria, Firmicutes, and Gemmatimonadetes (Fig 4C, Table S4). Similar communities have repeatedly been reported for arid and hyperarid soils and rocks (Angel & Conrad, 2013; Barberán et al., 2014; Lang-Yona et al., 2018). While cyanobacteria are typically the main primary producers in the soil and rock communities (Weber, Büdel, & Belnap, 2016), recent studies showed that other autotrophs may also contribute significantly to the energy balance of these biofilms (Ji et al., 2017).

The BRCs of the two rock types differed in the relative abundance and composition of major phyla. Most notably, Proteobacteria were significantly more dominant in the hyperarid compared to the arid samples ($P = 0.02$) comprising on average 21% and 44% of the community in the limestone and dolomite BRC, respectively. In contrast, the Actinobacteria showed an opposite trend ($P = 0.03$) comprising on average 42% and 21% of the community in the limestone and dolomite BRC, respectively. The two BRCs also differed in their composition of Firmicutes, Gemmatimonadetes and Chloroflexi ($P < 0.03$; Fig 4C, Table S4).

The soil samples generally showed similar trends on the gross taxonomic level as their respective BRC samples. While none of the phyla differed significantly between the hyperarid BRC and the soil, the phyla Deinococcus–Thermus, Acidobacteria, Firmicutes, and Gemmatimonadetes significantly differed between limestone BRC and the surrounding arid soil ($P < 0.04$; Table S4). Lastly, the arid and hyperarid dust samples were dominated by members of the Proteobacteria, with other phyla comprising only a minor fraction of the community (with a notable exception of Bacteroidetes that dominated one of the dust samples). However, these differences were not significant, probably due to the small sample size (Table S4).

Despite the general similarities in community composition between samples on the phylum level, many of the OTUs found in each sample were unique to the BRC, soil or dust as evident by the ternary diagrams (Fig. 4D). Direct analysis of the differences in the OTUs detected 130 (10%) differentially abundant OTUs in the dolomite BRC and 74 (6%) differentially abundant OTUs in the limestone BRC (Fig. S2). Similarly, several differentially abundant OTUs were also detected when comparing the BRCs to their respective soil and dust samples. However, these differentially abundant OTUs were fewer, probably due to the small dust sample size (Fig. S2).

The BRC bacterial communities were previously described (Kuhlman et al., 2006; Lang-Yona et al., 2018; Wong, Lacap, et al., 2010; Wong, Lau, et al., 2010) but their origin and role in geomorphological processes were not considered. Our results suggest that despite the similarity in morphology and magnitude of rock weathering features in the arid limestone and hyperarid dolomites, the two BRCs harboured distinct microbial communities, differing in over 16% of the OTUs and their composition at the phylum level. Moreover, despite the spatial proximity and continuous interaction between the limestone and dolomite surface to their respective surrounding soils and dust particles, the bacterial communities of the BRCs were distinct. The abilities of bacteria to disperse, settle and persist in a given location could be an important factor resulting in the biogeographic patterns observed here. The difference between arid and hyperarid soil communities could result from the local contribution of aeolian material that might affect the loess soil diversity (Crouvi, Amit, Enzel, Porat, & Sandler, 2008). Alternatively, the hyperarid site experience slow pedological processes while arid soil formation was enhanced (Amit et al., 2011) resulting in disparate bacterial communities. The three matrices (BRC, soil and settled dust) studied here sparsely shared their bacterial communities and specifically, the BRC community had little in common with the soil or dust communities (Fig 4). This demonstrates the ecological filtering effect of the rock surfaces, which imposes unique abiotic challenges on the microbes living on it (Horner-

285 Devine & Bohannan, 2006). This also suggests that the BRCs cannot be regarded as passive deposits of
286 microbial cells originating from the surrounding soil or dust, but rather it is a specific subset of
287 adapted microbes that can persist and form a biofilm under these unique conditions.

288 ***The role of BRC in arid rock weathering - synthesis***

289 Honeycomb weathering patterns are prevalent worldwide and are found in both humid and dry
290 ecosystems. According to contemporary models, this form of weathering is the result of the
291 transport of dissolved salts through the rock and their eventual crystallisation in surface pores,
292 leading to fractures and eventual flaking of rock material (Rodriguez-Navarro, Doehne, & Sebastian,
293 1999). In this study, we found that weathering patterns and magnitude are similar on rocks from
294 both arid and hyperarid sites, despite the differences in precipitation and lithologies. In arid and
295 hyperarid regions, BRCs were shown to form once the rock is exposed to the atmosphere (Pointing
296 & Belnap, 2012). A developed crust of biological origin was microscopically and isotopically
297 apparent on all weathered rocks and was shown to be supported by EPS (Fig. 2). Similar to
298 weathering magnitude, the BRCs showed no observable differences in form or depth despite the
299 different aridity and lithology. Both BRCs comprised bacterial taxa that are typical for xeric
300 environments (Pointing & Belnap, 2012) and included many heterotrophs but also dominant
301 phototrophs or otherwise autotrophic members (Fig. 4). The two BRCs did differ in their bacterial
302 communities at the OTU and higher taxonomical levels, demonstrating a discrepancy between
303 composition and function. The BRC communities also differed from their surrounding soil and dust,
304 indicative of the specialism of the colonising taxa to rock environment. In the absence of
305 mineralized networks or case hardening (i.e., addition of cementing agent to rock matrix material)
306 we conclude that calcrete and dolocrete were formed through the colonisation of microorganisms
307 and the secretion of EPS, serving as a thin biofilm (Brantley et al., 2011; Weber et al., 2016).

Our results further suggest that this biogenic layer mitigates evaporation and reduces water transport, hence alleviating salt crystallisation pressure in the rock pours (Scherer, 2004). Crystallization of calcium sulphate and sodium chloride solutions, which are abundant in these soils, was shown to build pressure within pores and stress rocks (Scherer, 2004; Sperling & Cooke, 1985). This process is enhanced under low relative humidity and rapid evaporation and compromises the durability of the rocks (Rodriguez-Navarro & Doehne, 1999; Rodriguez-Navarro, Rodriguez-Gallego, Chekroun, & Gonzalez-Muñoz, 2003). Our results suggest that the presence of BRC decreases evaporation rates (Fig 3) and thus attenuate the crystallisation pressure and reduces damage to the rocks. Moreover, the BRC may also stabilise the rock following exfoliation preserving the weathered structure.

Arid weathering features, which lead to debris formation result from a dynamic balance between the erosive salt forces and the mitigating effects of the BRC. The role of microbial biofilms in the protection of surfaces from mineral weathering was extensively studied for biomineralisation and sedimentation processes (Adams, Palmer, & Staley, 1992; Dupraz et al., 2009). Yet, the role of BRC in weathering processes under atmospheric conditions in the desert has not been considered before. We propose that microbial colonisation of mineral surfaces protects the rocks from weathering by mitigating salt crystallisation and stabilising the weathered front. Rock weathering processes are typically believed to be controlled at different scales ranging from the climatic scale, down to local conditions at the site and eventually the microscale (Smith, 2009; Sperling & Cooke, 1985; Heather A Viles, 2001). The results presented here suggest that in arid environments, microscale conditions determine the magnitude of weathering that shape the landscape.

Materials and Methods

Study site

We focused on two sites in the Negev Desert, Israel: Sede-Boqer – an arid site and Uvda Valley – a hyperarid site (Fig. S1, Table 1). Both sites are rocky terrains underlined predominantly by carbonate rock slopes consisting of limestone, dolomite, chalk, marl, clay and chert from the Cretaceous to Eocene age. Our analyses compared samples from the limey Turonian age Shivta Formation located in the arid region with samples from the dolomitic Turonian age Gerofit Formation located in the hyperarid environment. The Negev Desert, Israel, maintains arid to hyperarid conditions since the Holocene and has an aridity index (P/PET) of 0.05-0.005 (Amit et al., 2010; Bruins, 2012) similar to other arid and hyperarid areas worldwide, e.g., the Namib and Atacama Deserts (Azua-Bustos, Urrejola, & Vicuña, 2012; Viles & Goudie, 2007). The long-term aridity of the Negev Desert makes it a reliable site for testing the cross-influence between BRCs and geological substrates.

Field sampling

Twenty-four rock samples were collected along rocky slopes facing northward, comprising: twelve limestone samples from the limey Turonian age Shivta Formation at the arid site (30.88N34.78E, WGS 84 Grid; samples named: SB 1-12) and twelve dolomite samples from limey-dolomitic Turonian age Gerofit Formation at the hyperarid site (29.94N34.97E, WGS 84 Grid; samples named: UV 1-12) during November and December, 2014. Concomitantly, six soil samples (ca. 500 g each) were collected, half from the arid (named: SBSoil 1-3) and a half from the hyperarid (named: UVSoil 1-12) sites. Each rock or soil sample is a composite of four sub-samples that were pooled and homogenised in the lab.

We also collected settled dust samples using glass beads traps (Goossens & Rajot, 2008). The traps were placed on December 2013 and collected three months later in the arid (samples named: SBDust 1-2) and hyperarid (samples named: UVDust 1-2) sites. Each dust sample was a composite of two sub-samples that were pooled and homogenised in the lab.

Geological analyses

The geological methods used in this study are based on direct field observations and detailed characterisation of the subjected lithologies (i.e., Limestone and Dolomite) which included morphology (thin sections), mineral components [X-ray powder diffraction (XRD)], porosity and permeability (Automatic Gas Permeameter Porosimeter), and elastic properties (Schmidt hammer): Petrographic thin sections, 30 µm thick, were prepared for each lithology to test the main components in both the BRC and host rocks examined under a light microscope (Zeiss, Oberkochen, Germany). XRD analysis of mineral components (Sandler et al., 2015) was conducted on the BRC and host rocks using three replicates each. Powdered samples were scanned using X'Pert^3 Powder diffractometer equipped with a PIXcel detector (Panalytical Malvern, Almelo, Netherlands). Scanning range was: 3 – 70° 2θ, step size 0.013°, speed 70.1 s per step. Total effective porosity (ϕ) and permeability (k) tests (Scherer, 1999) were performed using Automatic Gas Permeameter Porosimeter (Core Laboratories, Houston, Texas, USA) on twelve rock core cylinder samples, with 18.5 mm radius and 26.5 mm height. Six samples were taken from each lithology, each set of six samples were prepared in two orthogonal directions providing the normal to bedding and parallel to bedding. Before testing porosity and permeability, samples were oven dried at a temperature of 110°c for 24 h. Schmidt hammer (Lassen, Aarhus, Denmark) tests were applied in the field (Goudie, 2016; Viles, Goudie, Grab, & Lalley, 2011). Twenty measurements were carried out for each lithology.

FTIR and stable isotope analysis

Fourier transform infrared spectroscopy (FTIR) analysis was conducted for testing the presence of extracellular polymeric substances (EPS) on the rock surfaces while the host rock was used for comparison. The spectra were recorded using a Vertex 70 FTIR spectrometer (Bruker, Billerica, MA, USA) with a 4 cm^{-1} scan resolution. One to two mg of pulverised rock was taken from each sample (n = 2), and the spectra were measured twice collected over a wavenumber range 4000-600 cm^{-1}, and a baseline correction was carried out. The spectral absorption bands, indicative for EPS, were identified according to published information (Ferrando et al., 2018).

For $\delta^{13}C$ and $\delta^{18}O$ analysis, 1-2 mg of rock surface powder (i.e., calcite or dolomite) was obtained using a Microdrill (Dremel, Racine, WI, USA) along with a cross-section of the rock crust and its host rock. Four profiles measurements of $\delta^{13}C$ and $\delta^{18}O$ were performed on samples UVSL 5-6 from the hyperarid site and NWSH 1-2 from the arid site. Measurements (in duplicate) of $\delta^{18}O$-H_2O and $\delta^{13}C$-DIC were performed on gas source isotope ratio mass spectrometer (GS-IRMS; Thermo Fisher Scientific, Waltham, MA, USA) coupled to a Gas Bench II interface (Thermo) after CO_2 equilibration or CO_2 extraction by acidification for $\delta^{18}O$-H_2O and $\delta^{13}C$-DIC, respectively. The samples were calibrated against internal laboratory standards: Vienna Standard Mean Ocean Water (VSMOW) and carbonate standard NBS19. $\delta^{13}C$ values were also referenced against VSMOW and valued for carbonate relative to Vienna PeeDee Belemnite (VPDB) standard as previously described (Uemura et al., 2016) with SD of 0.1‰. All values are reported in per-mil (‰).

Desiccation experiment

To test the effect of biological rock crusts on water transport rates in the rock, clogging and desiccation experiments were performed on sixteen rock core cylinders from both lithologies (limestone and dolomite). Rock cylinders (⌀ 37 mm, 6.5 cm) were drilled using a rock core drill. Each

set of eight rock cores from the two different lithologies included four rock cores that were kept intact, and four rock cores that their BRC was mechanically removed using a diamond saw (Dremel, Racine, WI, USA) to a depth of 5 cm. Each cylinder was immersed in distilled water for 72 h, covered with epoxy (Devcon) and aluminium foil, leaving only the upper base of the crusted and bare cylinders uncovered to allow evaporation. The cylinders were then weighed (t=0), incubated in an oven dried at a temperature of 44 °C for 48 h and weighed every 2 h during the first 12 h and then every 6 h to determine the residual water content. Second-degree polynomial functions were fitted using function stats::lm to determine evaporation rates and compared using ANOVA in R.

DNA Extraction PCR amplification and sequencing

For DNA extraction from all rocks, the surface (ca. 100 cm^2) was scraped using a rasp (66-67 HRC hardness; Dieter Schmid, Berlin, Germany) that was cleaned with 70% technical-grade ethanol before each sampling. DNA was then extracted from 0.5 g of the homogenised sample using bead-beating in the presence of a CTAB buffer and phenol, according to a previously published extraction protocol (Angel, Claus, & Conrad, 2012). A 466-bp fragment of the *16S rRNA* gene was amplified using the universal bacterial primers 341F (CCTAYGGGRBGCASCAG) and 806R (GGACTACNNGGGTATCTAAT) flanking the V3 and V4 region (Klindworth et al., 2012). Library construction and sequencing were performed at a DNA Services Facility (University of Illinois at Chicago, USA) using a MiSeq sequencer (Illumina, San Diego, CA, USA) in the 2 × 250 cycle configuration (V2 regent kit). The raw sequencing data were deposited into the EMBL-ENA SRA database (https://www.ebi.ac.uk/ena/) and can be found under study accession PRJNA381483.

Sequence processing and analysis of bacterial communities

Paired reads generated by the MiSeq platform were quality filtered and clustered into OTUs using the UPARSE pipeline (Edgar, 2013), with modifications. Contig assembly was done using the

fastq_mergepairs command. Then, contigs were dereplicated with the derep_fullength command, and singleton sequences were removed. OTU centroids were then determined with the cluster_otus command (set at 3% radius). Abundances of OTUs were determined by mapping the filtered contigs (before dereplication, including singletons) to the OTU centroids using the usearch_global command (set at 0.97% identity). Following these steps, a total of ca. 1.4 G reads remained. OTU representatives were classified using mothur's implementation of a Naïve Bayesian sequence classifier (Schloss et al., 2009; Wang, Garrity, Tiedje, & Cole, 2007) against the SILVA 119 SSU NR99 database (Quast *et al.*, 2013). All downstream analyses were performed in R V3.4.4 (R Core Team, 2016). Data handling and manipulation were done using package phyloseq (McMurdie & Holmes, 2013). For alpha-diversity analysis, all samples were subsampled (rarefied) to the minimum sample size using bootstrap subsampling at 1000 iterations, to account for library size differences, while for beta-diversity analysis library size normalisation was done using GMPR (Chen et al., 2018). The ACE richness estimate (O'Hara, 2005) and Shannon's H diversity index were calculated using function EstimateR in the vegan package (Oksanen et al., 2018) and tested using ANOVA and Tukey HSD in the stats package. Variance partitioning and testing were done using PERMANOVA (McArdle & Anderson, 2001) function vegan::adonis using Horn-Morisita distances. Differences in phyla composition between the sample types were tested using the non-parametric Scheirer Ray Hare Test (Mangiafico, 2018; function rcompanion::scheirerRayHare) followed by the *post hoc* Mann-Whitney Test (function stats::wilcox.test) and FDR corrected using the Benjamini-Hochberg method (Ferreira & Zwinderman, 2006; function stats::p.adjust). Detection of differentially abundant OTUs was done using ALDEx2 (Fernandes et al., 2014). Plots were generated using packages ggplot2 (Wickham, 2016) and ggtern (Hamilton, 2017).

References

Adams, J. B., Palmer, F., & Staley, J. T. (1992). Rock weathering in deserts: Mobilization and concentration of ferric iron by microorganisms. *Geomicrobiology Journal*, *10*(2), 99–114. https://doi.org/10.1080/01490459209377910

Alonso-Zarza, A. M., & Wright, V. P. (2010). Chapter 5 Calcretes. In *Developments in Sedimentology* (Vol. 61, pp. 225–267). Elsevier. https://doi.org/10.1016/S0070-4571(09)06105-6

Alonso-Zarza, A. M., Bustamante, L., Huerta, P., Rodríguez-Berriguete, Á., & Huertas, M. J. (2016). Chabazite and dolomite formation in a dolocrete profile: An example of a complex alkaline paragenesis in Lanzarote, Canary Islands. *Sedimentary Geology*, *337*, 1–11. https://doi.org/10.1016/j.sedgeo.2016.02.018

Amit, R., Enzel, Y., Crouvi, O., Simhai, O., Matmon, A., Porat, N., … Gillespie, A. R. (2011). The role of the Nile in initiating a massive dust influx to the Negev late in the middle Pleistocene. *Geological Society of America Bulletin*, *123*(5–6), 873–889. https://doi.org/10.1130/B30241.1

Amit, R., Harrison, J. B. J., Enzel, Y., & Porat, N. (1996). Soils as a tool for estimating ages of Quaternary fault scarps in a hyperarid environment — the southern Arava valley, the Dead Sea Rift, Israel. *CATENA*, *28*(1–2), 21–45. https://doi.org/10.1016/S0341-8162(96)00028-8

Amit, R., Enzel, Y., Grodek, T., Crouvi, O., Porat, N., & Ayalon, A. (2010). The role of rare rainstorms in the formation of calcic soil horizons on alluvial surfaces in extreme deserts. *Quaternary Research*, *74*(02), 177–187. https://doi.org/10.1016/j.yqres.2010.06.001

Andrews, J. E., Singhvi, A. K., Kailath, A. J., Kuhn, R., Dennis, P. F., Tandon, S. K., & Dhir, R. P. (1998). Do stable isotope data from calcrete record Late Pleistocene monsoonal climate variation in the Thar Desert of India? *Quaternary Research*, *50*(03), 240–251. https://doi.org/10.1006/qres.1998.2002

Angel, R., Claus, P., & Conrad, R. (2012). Methanogenic archaea are globally ubiquitous in aerated soils and become active under wet anoxic conditions. *The ISME Journal*, *6*(4), 847–862. https://doi.org/10.1038/ismej.2011.141

Angel, R., & Conrad, R. (2013). Elucidating the microbial resuscitation cascade in biological soil crusts following a simulated rain event. *Environmental Microbiology*, *15*(10), 2799–2815. https://doi.org/10.1111/1462-2920.12140

Azua-Bustos, A., Urrejola, C., & Vicuña, R. (2012). Life at the dry edge: Microorganisms of the Atacama Desert. *FEBS Letters*, *586*(18), 2939–2945. https://doi.org/10.1016/j.febslet.2012.07.025

Barberán, A., Henley, J., Fierer, N., & Casamayor, E. O. (2014). Structure, inter-annual recurrence, and global-scale connectivity of airborne microbial communities. *Science of The Total Environment*, *487*, 187–195. https://doi.org/10.1016/j.scitotenv.2014.04.030

Brandmeier, M., Kuhlemann, J., Krumrei, I., Kappler, A., & Kubik, P. W. (2011). New challenges for tafoni research. A new approach to understand processes and weathering rates. *Earth Surface Processes and Landforms*, *36*(6), 839–852. https://doi.org/10.1002/esp.2112

Brantley, S. L., Megonigal, J. P., Scatena, F. N., Balogh-Brunstad, Z., Barnes, R. T., Bruns, M. A., … Yoo, K. (2011). Twelve testable hypotheses on the geobiology of weathering. *Geobiology*, *9*(2), 140–165. https://doi.org/10.1111/j.1472-4669.2010.00264.x

Brlek, M., & Glumac, B. (2014). Stable isotopic (δ13C and δ18O) signatures of biogenic calcretes marking discontinuity surfaces: a case study from Upper Cretaceous carbonates of central Dalmatia and eastern Istria, Croatia. *Facies*, *60*(3), 773–788. https://doi.org/10.1007/s10347-014-0403-7

Bruins, H. J. (2012). Ancient desert agriculture in the Negev and climate-zone boundary changes during average, wet and drought years. *Journal of Arid Environments*, *86*, 28–42. https://doi.org/10.1016/j.jaridenv.2012.01.015

Bruthans, J., Filippi, M., Slavík, M., & Svobodová, E. (2018). Origin of honeycombs: Testing the hydraulic and case hardening hypotheses. *Geomorphology*, *303*, 68–83. https://doi.org/10.1016/j.geomorph.2017.11.013

Bruthans, J., Soukup, J., Vaculikova, J., Filippi, M., Schweigstillova, J., Mayo, A. L., … Rihosek, J. (2014). Sandstone landforms shaped by negative feedback between stress and erosion. *Nature Geoscience*, *7*(8), 597–601. https://doi.org/10.1038/ngeo2209

Büdel, B., Weber, B., Kühl, M., Pfanz, H., Sültemeyer, D., & Wessels, D. (2004). Reshaping of sandstone surfaces by cryptoendolithic cyanobacteria: bioalkalization causes chemical weathering in arid landscapes. *Geobiology*, *2*(4), 261–268. https://doi.org/10.1111/j.1472-4677.2004.00040.x

Chen, L., Reeve, J., Zhang, L., Huang, S., Wang, X., & Chen, J. (2018). GMPR: A robust normalization method for zero-inflated count data with application to microbiome sequencing data. *PeerJ*, *6*, e4600. https://doi.org/10.7717/peerj.4600

Cooke, R. U. (1979). Laboratory simulation of salt weathering processes in arid environments. *Earth Surface Processes*, *4*(4), 347–359. https://doi.org/10.1002/esp.3290040405

Crouvi, O., Amit, R., Enzel, Y., Porat, N., & Sandler, A. (2008). Sand dunes as a major proximal dust source for late Pleistocene loess in the Negev Desert, Israel. *Quaternary Research*, *70*(2), 275–282. https://doi.org/10.1016/j.yqres.2008.04.011

Davey, M. E., & O'toole, G. A. (2000). Microbial biofilms: from ecology to molecular genetics. *Microbiology and Molecular Biology Reviews*, *64*(4), 847–867. https://doi.org/10.1128/MMBR.64.4.847-867.2000

Drews, A., Lee, C.-H., & Kraume, M. (2006). Membrane fouling - a review on the role of EPS. *Desalination*, *200*(1–3), 186–188. https://doi.org/10.1016/j.desal.2006.03.290

Dupraz, C., Reid, R. P., Braissant, O., Decho, A. W., Norman, R. S., & Visscher, P. T. (2009). Processes of carbonate precipitation in modern microbial mats. *Earth-Science Reviews*, *96*(3), 141–162. https://doi.org/10.1016/j.earscirev.2008.10.005

Edgar, R. C. (2013). UPARSE: highly accurate OTU sequences from microbial amplicon reads. *Nature Methods*, *10*(10), 996–998. https://doi.org/10.1038/nmeth.2604

Ehleringer, J. R., Cerling, T. E., & Helliker, B. R. (1997). C_4 photosynthesis, atmospheric CO_2, and climate. *Oecologia*, *112*(3), 285–299. https://doi.org/10.1007/s004420050311

Fernandes, A. D., Reid, J. N., Macklaim, J. M., McMurrough, T. A., Edgell, D. R., & Gloor, G. B. (2014). Unifying the analysis of high-throughput sequencing datasets: characterizing RNA-seq, 16S rRNA gene sequencing and selective growth experiments by compositional data analysis. *Microbiome*, *2*, 15. https://doi.org/10.1186/2049-2618-2-15

Ferrando, D., Toubiana, D., Kandiyote, N. S., Nguyen, T. H., Nejidat, A., & Herzberg, M. (2018). Ambivalent role of calcium in the viscoelastic properties of extracellular polymeric substances and the consequent fouling of reverse osmosis membranes. *Desalination*, *429*, 12–19. https://doi.org/10.1016/j.desal.2017.12.006

Ferreira, J. A., & Zwinderman, A. H. (2006). On the Benjamini–Hochberg method. *The Annals of Statistics*, *34*(4), 1827–1849. https://doi.org/10.1214/009053606000000425

Garcia-Pichel, F. (2006). Plausible mechanisms for the boring on carbonates by microbial phototrophs. *Sedimentary Geology*, *185*(3–4), 205–213. https://doi.org/10.1016/j.sedgeo.2005.12.013

Goossens, D., & Rajot, J. L. (2008). Techniques to measure the dry aeolian deposition of dust in arid and semi-arid landscapes: a comparative study in West Niger. *Earth Surface Processes and Landforms*, *33*(2), 178–195. https://doi.org/10.1002/esp.1533

Gorbushina, A. A. (2007). Life on the rocks. *Environmental Microbiology*, *9*(7), 1613–1631. https://doi.org/10.1111/j.1462-2920.2007.01301.x

Goudie, A. S., Viles, H. A., & Parker, A. G. (1997). Monitoring of rapid salt weathering in the central Namib Desert using limestone blocks. *Journal of Arid Environments*, *37*(4), 581–598. https://doi.org/10.1006/jare.1997.0297

Goudie, A. S. (2016). Quantification of rock control in geomorphology. *Earth-Science Reviews*, *159*, 374–387. https://doi.org/10.1016/j.earscirev.2016.06.012

Goudie, A. S., Wright, E., & Viles, H. A. (2002). The roles of salt (sodium nitrate) and fog in weathering: a laboratory simulation of conditions in the northern Atacama Desert, Chile. *CATENA*, *48*(4), 255–266. https://doi.org/10.1016/S0341-8162(02)00028-0

Goudie, A.S. (1996). Organic agency in calcrete development. *Journal of Arid Environments*, *32*(2), 103–110. https://doi.org/10.1006/jare.1996.0010

Groom, K. M., Allen, C. D., Mol, L., Paradise, T. R., & Hall, K. (2015). Defining tafoni: Re-examining terminological ambiguity for cavernous rock decay phenomena. *Progress in Physical Geography*, *39*(6), 775–793. https://doi.org/10.1177/0309133315605037

Hamilton, N. (2017). *ggtern: An Extension to "ggplot2", for the Creation of Ternary Diagrams*. Retrieved from https://CRAN.R-project.org/package=ggtern

Horner-Devine, M. C., & Bohannan, B. J. M. (2006). Phylogenetic clustering and overdispersion in bacterial communities. *Ecology*, *87*(sp7), S100–S108. https://doi.org/10.1890/0012-9658(2006)87[100:PCAOIB]2.0.CO;2

Huinink, H. P., Pel, L., & Kopinga, K. (2004). Simulating the growth of tafoni. *Earth Surface Processes and Landforms*, *29*(10), 1225–1233. https://doi.org/10.1002/esp.1087

Ji, M., Greening, C., Vanwonterghem, I., Carere, C. R., Bay, S. K., Steen, J. A., … Ferrari, B. C. (2017). Atmospheric trace gases support primary production in Antarctic desert surface soil. *Nature*. https://doi.org/10.1038/nature25014

Jiang, W., Saxena, A., Song, B., Ward, B. B., Beveridge, T. J., & Myneni, S. C. B. (2004). Elucidation of functional groups on gram-positive and gram-negative bacterial surfaces using infrared spectroscopy, 10.

Klindworth, A., Pruesse, E., Schweer, T., Peplies, J., Quast, C., Horn, M., & Glockner, F. O. (2012). Evaluation of general 16S ribosomal RNA gene PCR primers for classical and next-generation sequencing-based diversity studies. *Nucleic Acids Research*, *41*(1), e1–e1. https://doi.org/10.1093/nar/gks808

Kuhlman, K. R., Fusco, W. G., La Duc, M. T., Allenbach, L. B., Ball, C. L., Kuhlman, G. M., … Crawford, R. L. (2006). Diversity of microorganisms within rock varnish in the Whipple Mountains, California. *Applied and Environmental Microbiology*, *72*(2), 1708–1715. https://doi.org/10.1128/AEM.72.2.1708-1715.2006

Lang-Yona, N., Maier, S., Macholdt, D. S., Müller-Germann, I., Yordanova, P., Rodriguez-Caballero, E., … Weber, B. (2018). Insights into microbial involvement in desert varnish formation retrieved from metagenomic analysis. *Environmental Microbiology Reports*, *10*(3), 264–271. https://doi.org/10.1111/1758-2229.12634

Lebre, P. H., Maayer, P. D., & Cowan, D. A. (2017). Xerotolerant bacteria: surviving through a dry spell. *Nature Reviews Microbiology*, *15*(5), 285–296. https://doi.org/10.1038/nrmicro.2017.16

Makhalanyane, T. P., Valverde, A., Birkeland, N.-K., Cary, S. C., Marla Tuffin, I., & Cowan, D. A. (2013). Evidence for successional development in Antarctic hypolithic bacterial communities. *The ISME Journal*, *7*(11), 2080–2090. https://doi.org/10.1038/ismej.2013.94

576 Makhalanyane, T. P., Valverde, A., Gunnigle, E., Frossard, A., Ramond, J.-B., & Cowan, D. A. (2015). Microbial
577 ecology of hot desert edaphic systems. *FEMS Microbiology Reviews*, *39*(2), 203–221.
578 https://doi.org/10.1093/femsre/fuu011
579 Mangiafico, S. (2018). *rcompanion: functions to support extension education program evaluation*. Retrieved
580 from https://CRAN.R-project.org/package=rcompanion
581 McArdle, B. H., & Anderson, M. J. (2001). Fitting multivariate models to community data: a comment on
582 distance-based redundancy analysis. *Ecology*, *82*(1), 290–297. https://doi.org/10.1890/0012-
583 9658(2001)082[0290:FMMTCD]2.0.CO;2
584 McBride, E. F., & Picard, M. D. (2004). Origin of honeycombs and related weathering forms in Oligocene
585 Macigno Sandstone, Tuscan coast near Livorno, Italy. *Earth Surface Processes and Landforms*, *29*(6),
586 713–735. https://doi.org/10.1002/esp.1065
587 McIlroy de la Rosa, J. P., Warke, P. A., & Smith, B. J. (2014). The effects of lichen cover upon the rate of
588 solutional weathering of limestone. *Geomorphology*, *220*, 81–92.
589 https://doi.org/10.1016/j.geomorph.2014.05.030
590 McMurdie, P. J., & Holmes, S. (2013). phyloseq: an R package for reproducible interactive analysis and
591 graphics of microbiome census data. *PLOS ONE*, *8*(4), e61217.
592 https://doi.org/10.1371/journal.pone.0061217
593 Mora, C. I., Driese, S. G., & Seager, P. G. (1991). Carbon dioxide in the Paleozoic atmosphere: Evidence from
594 carbon-isotope compositions of pedogenic carbonate. *Geology*, *19*(10), 1017.
595 https://doi.org/10.1130/0091-7613(1991)019<1017:CDITPA>2.3.CO;2
596 Mustoe, G. E. (1983). Cavernous weathering in the Capitol Reef Desert, Utah. *Earth Surface Processes and*
597 *Landforms*, *8*(6), 517–526. https://doi.org/10.1002/esp.3290080603
598 Mustoe, G. E. (2010). Biogenic origin of coastal honeycomb weathering. *Earth Surface Processes and*
599 *Landforms*, *35*(4), 424–434. https://doi.org/10.1002/esp.1931
600 O'Hara, R. B. (2005). Species richness estimators: how many species can dance on the head of a pin? *Journal*
601 *of Animal Ecology*, *74*(2), 375–386. https://doi.org/10.1111/j.1365-2656.2005.00940.x
602 Oksanen, J., Blanchet, F. G., Friendly, M., Kindt, R., Legendre, P., McGlinn, D., … Wagner, H. (2018). *vegan:*
603 *community ecology package*. Retrieved from https://CRAN.R-project.org/package=vegan
604 Or, D., Smets, B. F., Wraith, J. M., Dechesne, A., & Friedman, S. P. (2007). Physical constraints affecting
605 bacterial habitats and activity in unsaturated porous media – a review. *Advances in Water Resources*,
606 *30*(6–7), 1505–1527. https://doi.org/10.1016/j.advwatres.2006.05.025
607 Pointing, S. B., & Belnap, J. (2012). Microbial colonization and controls in dryland systems. *Nature Reviews*
608 *Microbiology*, *10*(8), 551–562. https://doi.org/10.1038/nrmicro2831

609 Roberson, E. B., & Firestone, M. K. (1992). Relationship between desiccation and exopolysaccharide
610 production in a soil Pseudomonas sp. *Applied and Environmental Microbiology*, *58*(4), 1284–1291.
611 Rodriguez-Navarro, C., & Doehne, E. (1999). Salt weathering: influence of evaporation rate, supersaturation
612 and crystallization pattern. *Earth Surface Processes and Landforms*, *24*(3), 191–209.
613 https://doi.org/10.1002/(SICI)1096-9837(199903)24:3<191::AID-ESP942>3.0.CO;2-G
614 Rodriguez-Navarro, C., Doehne, E., & Sebastian, E. (1999). Origins of honeycomb weathering: The role of salts
615 and wind. *Geological Society of America Bulletin*, *111*(8), 1250–1255. https://doi.org/10.1130/0016-
616 7606(1999)111<1250:OOHWTR>2.3.CO;2
617 Rodriguez-Navarro, C., Rodriguez-Gallego, M., Chekroun, K. B., & Gonzalez-Muñoz, M. T. (2003).
618 Conservation of Ornamental Stone by Myxococcus xanthus-Induced Carbonate Biomineralization.
619 *Applied and Environmental Microbiology*, *69*(4), 2182–2193.
620 https://doi.org/10.1128/AEM.69.4.2182-2193.2003
621 Scherer, G. W. (2004). Stress from crystallization of salt. *Cement and Concrete Research*, *34*(9), 1613–1624.
622 https://doi.org/10.1016/j.cemconres.2003.12.034
623 Schloss, P. D., Westcott, S. L., Ryabin, T., Hall, J. R., Hartmann, M., Hollister, E. B., … Weber, C. F. (2009).
624 Introducing mothur: open-source, platform-independent, community-supported software for
625 describing and comparing microbial communities. *Applied and Environmental Microbiology*, *75*(23),
626 7537–7541. https://doi.org/10.1128/AEM.01541-09
627 Sheng, G. P., Yu, H. Q., & Li, X. Y. (2010). Extracellular polymeric substances (EPS) of microbial aggregates in
628 biological wastewater treatment systems: A review. *Biotechnology Advances*, *28*(6), 882–894.
629 https://doi.org/10.1016/j.biotechadv.2010.08.001
630 Shirshova, L. T., Ghabbour, E. A., & Davies, G. (2006). Spectroscopic characterization of humic acid fractions
631 isolated from soil using different extraction procedures. *Geoderma*, *133*(3–4), 204–216.
632 https://doi.org/10.1016/j.geoderma.2005.07.007
633 Shtober-Zisu, N., Amasha, H., & Frumkin, A. (2017). Inland notches: lithological characteristics and climatic
634 implications of subaerial cavernous landforms in Israel: Inland Notches: Lithological characteristics
635 and climatic implications. *Earth Surface Processes and Landforms*, *42*(12), 1820–1832.
636 https://doi.org/10.1002/esp.4135
637 Slavík, M., Bruthans, J., Filippi, M., Schweigstillová, J., Falteisek, L., & Řihošek, J. (2017). Biologically-initiated
638 rock crust on sandstone: Mechanical and hydraulic properties and resistance to erosion.
639 *Geomorphology*, *278*, 298–313. https://doi.org/10.1016/j.geomorph.2016.09.040
640 Smith, B. J. (1988). Weathering of superficial limestone debris in a hot desert environment. *Geomorphology*,
641 *1*(4), 355–367. https://doi.org/10.1016/0169-555X(88)90007-4

642 Smith, B. J. (2009). Weathering Processes and Forms. In A. J. Parsons & A. D. Abrahams (Eds.),
643 *Geomorphology of Desert Environments* (pp. 69–100). Dordrecht: Springer Netherlands.
644 https://doi.org/10.1007/978-1-4020-5719-9_4
645 Smith, B. J., Warke, P. A., McGreevy, J. P., & Kane, H. L. (2005). Salt-weathering simulations under hot desert
646 conditions: agents of enlightenment or perpetuators of preconceptions? *Geomorphology*, *67*(1–2),
647 211–227. https://doi.org/10.1016/j.geomorph.2004.03.015
648 Sperling, C. H. B., & Cooke, R. U. (1985). Laboratory simulation of rock weathering by salt crystallization and
649 hydration processes in hot, arid environments. *Earth Surface Processes and Landforms*, *10*(6), 541–
650 555. https://doi.org/10.1002/esp.3290100603
651 Šťovíček, A., Kim, M., Or, D., & Gillor, O. (2017). Microbial community response to hydration-desiccation
652 cycles in desert soil. *Scientific Reports*, *7*, 45735. https://doi.org/10.1038/srep45735
653 Sweeting, M. M., & Lancaster, N. (1982). Solutions and wind erosion forms on limestone in the Central Namib
654 Desert. *Z. Geomorphology N. F.*, *26*(2), 197–207.
655 Uemura, R., Nakamoto, M., Asami, R., Mishima, S., Gibo, M., Masaka, K., … Shen, C.-C. (2016). Precise oxygen
656 and hydrogen isotope determination in nanoliter quantities of speleothem inclusion water by cavity
657 ring-down spectroscopic techniques. *Geochimica et Cosmochimica Acta*, *172*, 159–176.
658 https://doi.org/10.1016/j.gca.2015.09.017
659 Vaks, A., Bar-Matthews, M., Matthews, A., Ayalon, A., & Frumkin, A. (2010). Middle-Late Quaternary
660 paleoclimate of northern margins of the Saharan-Arabian Desert: reconstruction from speleothems
661 of Negev Desert, Israel. *Quaternary Science Reviews*, *29*(19–20), 2647–2662.
662 https://doi.org/10.1016/j.quascirev.2010.06.014
663 Viles, H. (1995). Ecological perspectives on rock surface weathering: Towards a conceptual model.
664 *Geomorphology*, *13*(1–4), 21–35. https://doi.org/10.1016/0169-555X(95)00024-Y
665 Viles, H. (2005). Self-organized or disorganized? Towards a general explanation of cavernous weathering.
666 *Earth Surface Processes and Landforms*, *30*(11), 1471–1473. https://doi.org/10.1002/esp.1287
667 Viles, H., Goudie, A., Grab, S., & Lalley, J. (2011). The use of the Schmidt Hammer and Equotip for rock
668 hardness assessment in geomorphology and heritage science: a comparative analysis. *Earth Surface*
669 *Processes and Landforms*, *36*(3), 320–333. https://doi.org/10.1002/esp.2040
670 Viles, H.A., & Goudie, A. S. (2007). Rapid salt weathering in the coastal Namib Desert: Implications for
671 landscape development. *Geomorphology*, *85*(1–2), 49–62.
672 https://doi.org/10.1016/j.geomorph.2006.03.025
673 Viles, H. A. (2001). Scale issues in weathering studies. *Geomorphology*, *41*(1), 63–72.
674 https://doi.org/10.1016/S0169-555X(01)00104-0

675 Viles, H. A. (2008). Understanding dryland landscape dynamics: do biological crusts hold the key? *Geography*
676 *Compass*, *2*(3), 899–919. https://doi.org/10.1111/j.1749-8198.2008.00099.x
677 Viles, H. A. (2012). Microbial geomorphology: A neglected link between life and landscape. *Geomorphology*,
678 *157–158*, 6–16. https://doi.org/10.1016/j.geomorph.2011.03.021
679 Wang, Q., Garrity, G. M., Tiedje, J. M., & Cole, J. R. (2007). Naïve Bayesian classifier for rapid assignment of
680 rRNA sequences into the new bacterial taxonomy. *Applied and Environmental Microbiology*, *73*(16),
681 5261–5267. https://doi.org/10.1128/AEM.00062-07
682 Warscheid, T., & Braams, J. (2000). Biodeterioration of stone: a review. *International Biodeterioration &*
683 *Biodegradation*, *46*(4), 343–368. https://doi.org/10.1016/S0964-8305(00)00109-8
684 Weber, B., Büdel, B., & Belnap, J. (Eds.). (2016). *Biological Soil Crusts: An Organizing Principle in Drylands* (1st
685 ed. 2016 edition). New York, NY: Springer.
686 Wickham, H. (2016). *ggplot2: Elegant Graphics for Data Analysis*. New York, USA: Springer-Verlag. Retrieved
687 from http://ggplot2.org
688 Wong, F. K. Y., Lacap, D. C., Lau, M. C. Y., Aitchison, J. C., Cowan, D. A., & Pointing, S. B. (2010). Hypolithic
689 microbial community of quartz pavement in the high-altitude tundra of Central Tibet. *Microbial*
690 *Ecology*, *60*(4), 730–739. https://doi.org/10.1007/s00248-010-9653-2
691 Wong, F. K. Y., Lau, M. C. Y., Lacap, D. C., Aitchison, J. C., Cowan, D. A., & Pointing, S. B. (2010). Endolithic
692 microbial colonization of limestone in a high-altitude arid environment. *Microbial Ecology*, *59*(4),
693 689–699. https://doi.org/10.1007/s00248-009-9607-8
694 Wright, D. T., & Wacey, D. (2004). Sedimentary dolomite: a reality check. *Geological Society, London, Special*
695 *Publications*, *235*(1), 65–74. https://doi.org/10.1144/GSL.SP.2004.235.01.03
696

Figure legends

Figure 1. A. Comparable weathering features in the exposed limestone and dolomite rocks on both sites as noted in field outcrops (hammer for scale, 30 cm long). **B.** Visual presence of a rock crust with similar thickness (3-6 mm) in both rock types. The crust's mineralogical composition matched that of the host rock. **C.** Thin-section analysis of the rocks showing lamination structure in the BRCs. Dashed lines indicate the interface between BRC host rocks. BRC's mineralogy includes micritic to microsparitic dolomitic or calcitic crystals.

Figure 2. A. Fourier Transform Infrared (FTIR) analysis of limestone (top) and dolomite (bottom) BRCs indicating the presence of extracellular polymeric substances (EPS) molecules through the distinctive peak ranging between 1020-1040 cm^{-1}, which was absent from the host rocks. **B.** Carbon and oxygen isotope-ratio depth profiles of the limestone (top) and dolomite (bottom) BRC's in comparison to their host rocks.

Figure 3. Desiccation of rock cores in the presence and absence of BRC as a function of time, following full hydration. The curves indicate a second-degree polynomial line fitting (all fitted curves were statistically significant from each other in ANOVA tests with P values < 0.01 and $R^2 > 0.95$).

Figure 4. Microbial community features of the BRCs, the surrounding soils and settled dust in the two studied sites. **A.** Comparison of the richness in the form of observed no. of OTUs (S obs.) and the predicted number of OTUs (ACE index), and a comparison of α-diversity (Shannon's H Index) between the different sample types. Identical lower-case letters indicate no statistical difference between groups in a Tukey's HSD test. **B.** Clustering of sample types using a PCoA ordination based on Horn-Morisita distance matrix. Identical lower-case letters indicate no statistical difference

721 between groups in a pairwise PERMANOVA test. Ellipses denote 95% confidence intervals around
722 the arid and hyperarid samples assuming multivariate normal distribution. **C.** Composition of
723 bacterial phyla in the different sample types (see Table S4 for results of statistical tests in the
724 relative abundance of different phyla between sample types). **D.** Relative contribution of each
725 bacterial OTU to the community composition of each sample type. Top – arid site, bottom –
726 hyperarid site (see Figure S2 for statistical detection of preferentially abundant OTUs between each
727 sample-type pair.

728 ***Tables***

729 Table 1. Geological parameters of the subjected lithologies

Rock properties	Limestone (arid; Shivta Formation)			Dolomite (hyperarid; Gerofit Formation)		
	Dolomite	Calcium	Quartz	Dolomite	Calcium	Quartz
BRC mineralogy (%)	0	95	3	90	2	1
Host rock mineralogy (%)	0	95	0	95	0	1
Porosity (%)	13.5 ± 2.2			8.25 ± 1.3		
Permeability (miliDarcy)	0.1 – 3.8			0.05 – 0.41		
Surface penetration resistance (kg cm^{-1})	100 – 365			130 – 230		

730

731

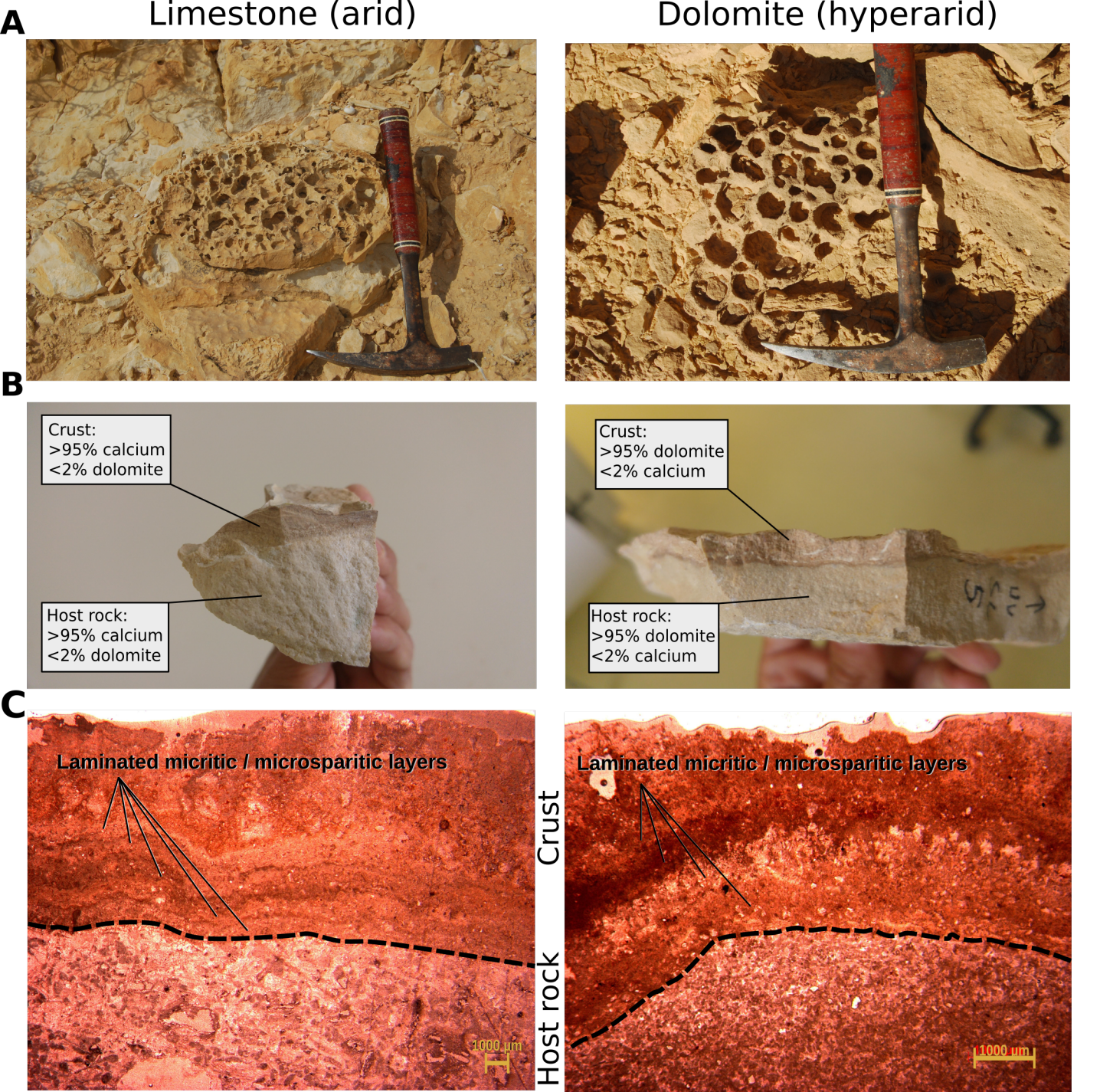
A
Limestone (arid)
Dolomite (hyperarid)
B
Crust:
>95% calcium
<2% dolomite
Host rock:
>95% calcium
<2% dolomite
Crust:
>95% dolomite
<2% calcium
Host rock:
>95% dolomite
<2% calcium
C
Laminated micritic / microsparitic layers
1000 µm
Crust
Host rock
Laminated micritic / microsparitic layers
1000 µm

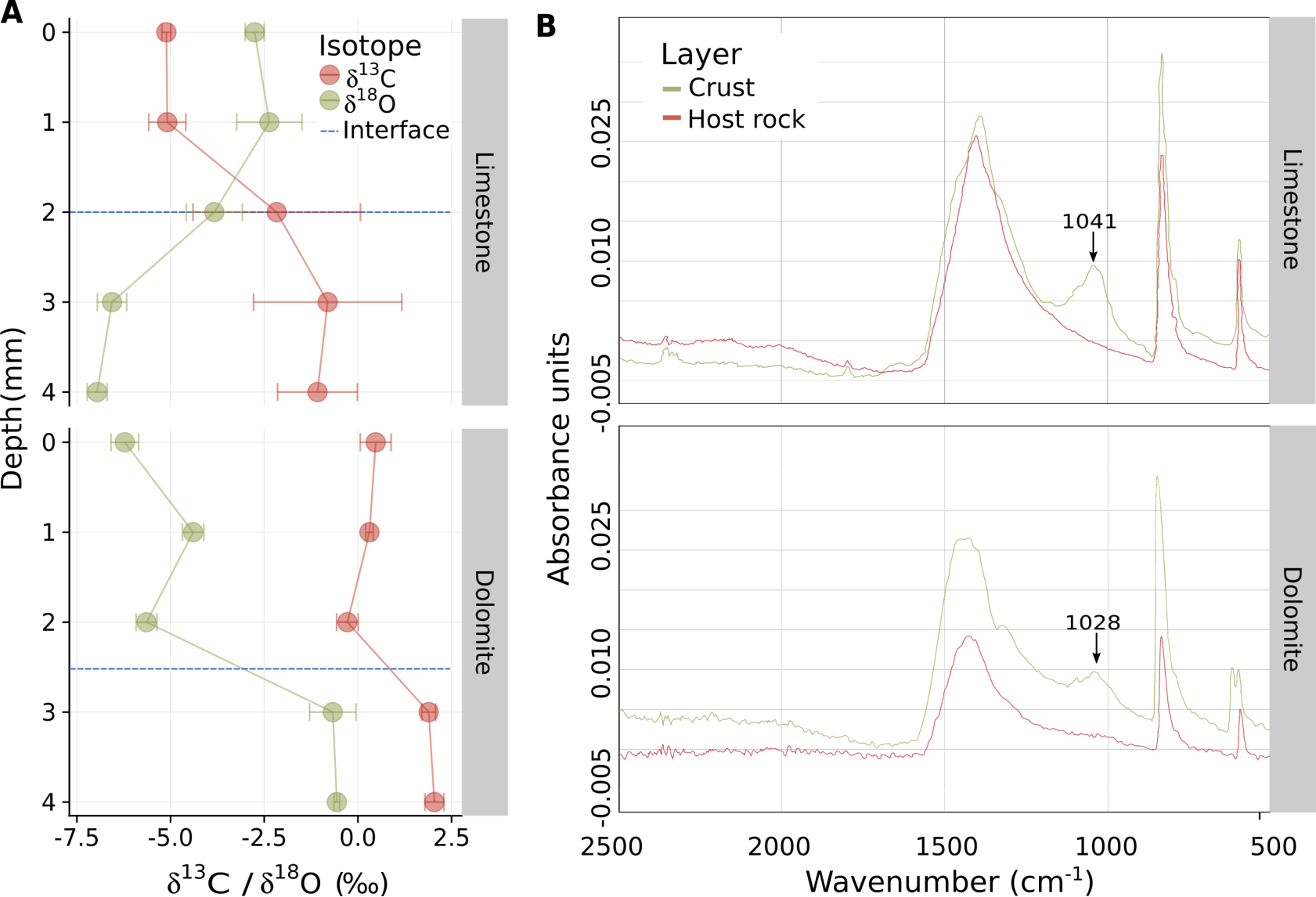
A
B
Isotope
δ13C
δ18O
Interface
Limestone
Dolomite
Depth (mm)
δ13C / δ18O (‰)
Layer
Crust
Host rock
Absorbance units
1041
1028
Wavenumber (cm-1)

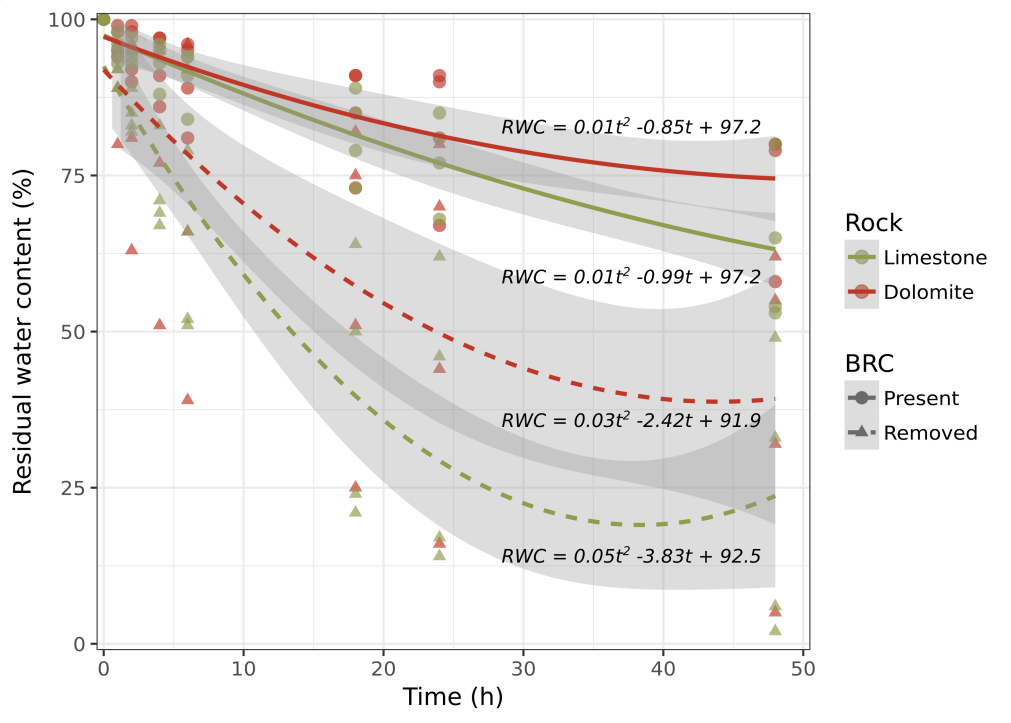
Residual water content (%)
100
75
50
25
0
0
10
20
30
40
50
Time (h)
RWC = 0.01t² -0.85t + 97.2
RWC = 0.01t² -0.99t + 97.2
RWC = 0.03t² -2.42t + 91.9
RWC = 0.05t² -3.83t + 92.5
Rock
Limestone
Dolomite
BRC
Present
Removed

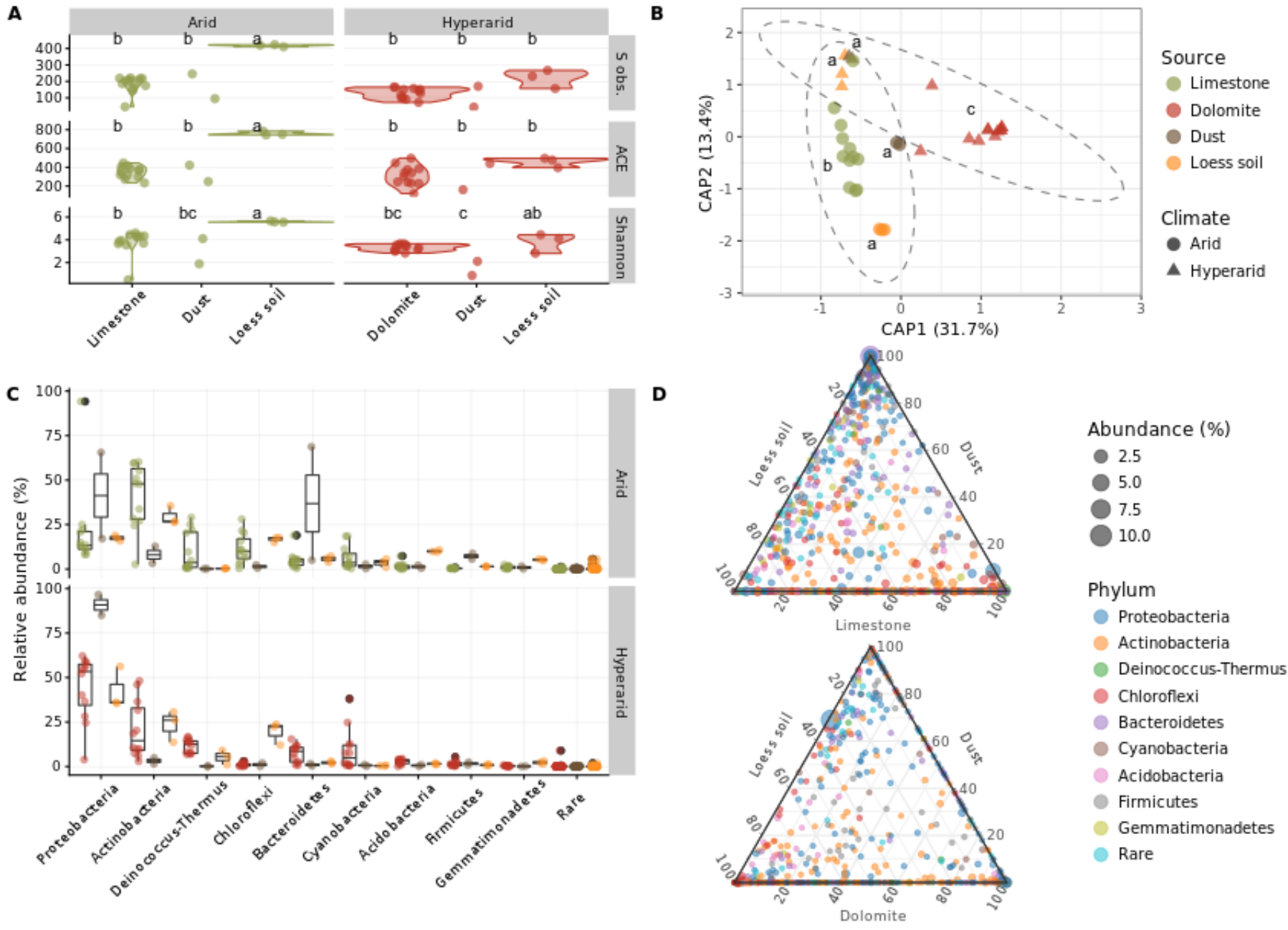
A
Arid
Hyperarid
S obs.
ACE
Shannon
Limestone
Dust
Loess soil
Dolomite
B
CAP2 (13.4%)
CAP1 (31.7%)
Source
Limestone
Dolomite
Dust
Loess soil
Climate
Arid
Hyperarid
C
Relative abundance (%)
Proteobacteria
Actinobacteria
Deinococcus-Thermus
Chloroflexi
Bacteroidetes
Cyanobacteria
Acidobacteria
Firmicutes
Gemmatimonadetes
Rare
D
Limestone
Dolomite
Abundance (%)
2.5
5.0
7.5
10.0
Phylum